

A STATISTICAL ANALYSIS ON THE “HEARTBEAT” BEHAVIOUR OF GRS 1915+105

SHAN-SHAN WENG¹, TING-TING WANG¹, JING-PING CAI¹, QI-RONG YUAN¹, WEI-MIN GU²

¹ Department of Physics and Institute of Theoretical Physics, Nanjing Normal University, Nanjing 210023, China and
² Department of Astronomy, Xiamen University, Xiamen, Fujian 361005, China

Draft version August 10, 2018

ABSTRACT

GRS 1915+105 has been active for more than 26 years since it was discovered in 1992. There are hundreds of *RXTE* pointed observations on this source, and the quasi-regular flares with a slow rise and a sharp decrease (i.e. the “heartbeat” state) were recorded in more than 200 observations. The connections among the disk/corona, jet, and the disk wind at the heartbeat state have been extensively studied. In this work, we firstly perform a statistical analysis on the light curves and the X-ray spectra to investigate this peculiar state. We calculate the parameters for heartbeat cycles, including the recurrence time, the maximum and the minimum count rate, the flare amplitude, and the cumulative radiation for each cycle. The recurrence time has a bimodal distribution ranging from ~ 20 to ~ 200 seconds. The minimum count rate increases with increasing recurrence time; while the maximum count rate remains nearly constant around 2 Crab. Fitting the averaged spectrum for each observation, we find the strong correlations among the recurrence time, the apparent inner radius of accretion disk (or the color correction factor), and the (non-thermal) X-ray luminosity. We suggest that the true inner edge of accretion disk might always extend to the marginally stable orbit, while the change in corona size should result in the observed correlations.

Keywords: accretion, accretion disks — black hole physics — X-rays: binaries — X-rays: stars — X-rays: individual (GRS 1915+105)

1. INTRODUCTION

The prototype microquasar GRS 1915+105, consisting of a black hole (BH) and a K-M III companion star (Greiner et al. 2001), was discovered by *GRANAT*/WATCH in 1992 (Castro-Tirado et al. 1992). Since then, the X-ray monitoring data reveal that it has remained bright during the last 26 years. The parallax distance is estimated at ~ 8.6 kpc, and the dynamical BH mass is measured as $\sim 12.4M_{\odot}$ with an orbital period of 34 days (Reid et al. 2014, and references therein). GRS 1915+105 exhibits fantastic phenomena and thus attracts a lot of attention to observations and accretion theories (e.g. Fender & Belloni 2004; Zdziarski et al. 2005; McClintock et al. 2006; Miller et al. 2013). Both the continuum spectral fitting and the relativistic disk reflection measurement indicate a rapidly spinning BH harbored in GRS 1915+105 (e.g. Zhang et al. 1997; Middleton et al. 2006; McClintock et al. 2006; Blum et al. 2009; Miller et al. 2013; Reid et al. 2014). The powerful jet with the apparent superluminal motion has been revealed (Mirabel & Rodríguez 1994), and whether the jets are driven by the BH spin energy is still in dispute (Fender et al. 2010; Narayan & McClintock 2012; Miller et al. 2013). The X-ray emissions show dramatic variability and quasi-periodic oscillation (QPO) in different time scales (e.g. Morgan et al. 1997; Belloni & Altamirano 2013; Zhang et al. 2015); therefore, GRS 1915+105 offers a remarkable laboratory for the investigation of accretion flows.

Analyzing a large set of *RXTE* observations, Belloni et al. (2000) classified 12 different variability patterns of X-ray emission, based on the count rate and

the hardness ratio characteristics. Two additional variability classes were proposed later by Klein-Wolt et al. (2002) and Hannikainen et al. (2005). Of these 14 classes of X-ray variability, the most intriguing is the ρ class, which displays the quasi-periodic bright flares, being analogous to the “heartbeat” behaviour. Therefore, the ρ class is also referred to as the heartbeat state, and it is only found in two BH X-ray binaries (XRBs), i.e. GRS 1915+105 and IGR J17091-3624 (e.g. Altamirano et al. 2011; Court et al. 2017). During the heartbeat state, the X-ray luminosity approaches the Eddington luminosity of the source at the peak of flares ($L_{\text{peak}} \sim 10^{39}$ erg/s). Thus, it provides an opportunity for us to study the accretion flows being close to the Eddington limit, which are extremely rudimentary.

Both the spectral and timing properties of heartbeat state have been extensively studied, and the connections among disk/corona, jet, and disk wind have been investigated in many papers (e.g. Neilsen et al. 2011; Yan et al. 2017, 2018). But to date, there is a lack of statistical analysis on this peculiar state. In this work, we investigate the light curves and the spectra of heartbeat state by using the full set of *RXTE* and search the correlations among the different parameters (Section 2). We present our results in Section 3 and explore the accretion theories at high luminosities close to the Eddington limit with the obtained relationships in Section 4.

2. DATA REDUCTION

The Rossi X-ray Timing Explorer Mission (*RXTE*, December 1995 – January 2012) carries three instruments, the Proportional Counter Array (PCA), the High Energy X-ray Timing Experiment, and the All-Sky Monitor. The primary scientific objectives of *RXTE* are to determine the origin of rapid variation from astronomical

X-ray sources. During its 16 years of science operations, *RXTE* visited GRS 1915+105 frequently (~ 1800 times). In this Paper, our study relies on two standard mode data from the PCA. The Standard 1 mode data have a time resolution of 0.125 seconds allowing us to depict the light curve profile at the heartbeat state; however, they do not have energy information for a spectral fitting¹. Alternatively, the Standard 2 mode data have 129 energy channels covering the full range of the PCA detectors, but the time resolution of 16 seconds is comparable to the heartbeat cycle, that is not fine enough for the timing analysis. Thus, we use the Standard 1 mode data for the timing study and the Standard 2 mode data for the time-averaged spectral fitting.

Different PCUs were active at different times due to some of the PCUs suffered breakdown and tripped off. In our temporal analysis, we adopt the standard products of the Standard 1 mode data, which are normalized to 1 PCU. Since the light curves of GRS 1915+105 could show chaotic variability at a short time scale, we smooth them with a span of 2 seconds in order to reduce these substructures. The light curves are further normalized to the quasi-simultaneous count rate of the Crab Nebula². It is worth to note that different flare classifications have been introduced by different groups (e.g. Yadav et al. 1999; Belloni et al. 2000; Massaro et al. 2010). Massaro et al. (2010) applied the Fourier and wavelet analysis to define the ρ class, which could show regular and irregular variational patterns. Alternatively, the irregular flares was classified as the κ class, and the regular flares was defined as the μ or ρ classes in Belloni et al. (2000) according to the properties of the count rate and the X-ray colors. In this paper, we adopt the classification in Belloni et al. (2000). That is, the heartbeat state is referred to as the regular oscillation. We pick out 233 observations at the heartbeat state from all *RXTE* pointed data with the visual inspection. The exposure time for these data ranges from 0.4 to 16.5 kilo seconds. For some observations with short exposure, it is difficult to distinguish the ρ from μ and κ classes. Because of this, the number of observation is slightly difference from those reported in Neilsen et al. (2012) (242 observations in their paper).

The start time of oscillation (T_{start}) is identified when the count rate reaches the maxima in the interval of $[T_{\text{start}} - \Delta T, T_{\text{start}} + \Delta T]$, where ΔT is about 10%-30% of the recurrence time. That is, we search the maxima by using a running box with a size of $\sim 20\%$ of the recurrence time. Note that the derived T_{start} is not affected by the size of running box. It is very rare that the recurrence time of some oscillation is almost twice as long as the neighbors. In this case, the local maxima would be reported by the automated process, and we make double check visually to screen out the local maxima. Once the T_{start} is fixed, we introduce the structure parameters to characterize the light curves as follows: The maximum (i.e. the peak, C_{max}) and minimum (C_{min}) count rates during each cycle; The recurrence time (T_{rec}) is defined as the time interval between two peaks; The amplitude of flares is calculated as the ratio of C_{max} and C_{min} ($C_{\text{max}}/C_{\text{min}}$); The fluence is referred to as the cu-

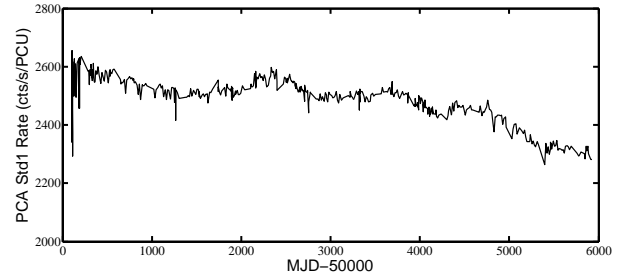


Figure 1. *RXTE* mission long PCA light curve from Crab. Because of the degradation of detection efficiency, the count rate recorded in the Standard 1 mode data decreased from ~ 2600 cts/s/PCU to ~ 2300 cts/s/PCU.

mulative X-ray radiation during each cycle. Because the flare property is quite stable within an individual observation, we calculate the mean value of these parameters for every observation, and assign the standard deviations to the errors of parameters.

The exposure time of an individual pointing is much longer than T_{rec} , and one observation contains at least 3 heartbeat cycles. Therefore, the spectrum from a full observation can be treated as the phase averaged spectrum for the following analysis. We extract the X-ray spectrum with the Standard 2 mode data from the top layer of PCU2, which operated during all the observations. The data are filtered with standard criteria. The background files are produced with the bright source background model by using the task `pcabackest`, and the response file is created with the PCA response generator `PCARMF v11.7`. A systematic error of 0.5% as recommended by the PCA team is added in the spectral modelling. Following the work in Neilsen et al. (2011), we fit the deadtime corrected spectrum in the 3–30 keV with the empirical model consisting of a multi-color disk, a power-law component plus a high-energy cutoff ($tbabs*highcut*(diskbb+powerlaw)$ in XSPEC, Arnaud 1996). The neutral hydrogen column density is fixed to $5 \times 10^{22} \text{ cm}^{-2}$ (Lee et al. 2002; Zoghbi et al. 2016). The yielded reduced χ^2 centered around ~ 0.74 with a minima of 0.39 and a maxima of 1.27. No correlation between the reduced χ^2 and other spectral parameters is found. The unabsorbed fluxes in 3–30 keV are estimated with the convolution model `cflux`, and the errors for all spectral parameters are calculated in 68.3% confidence level.

3. RESULTS

The goal of our work is to search the correlation between the heartbeat parameters and to achieve the knowledge on the accretion at high luminosity close to the Eddington limit.

3.1. Light curve analysis

The distributions of the time-varying parameters are plotted in Figures 2. The recurrence time ranges from ~ 20 to ~ 200 seconds, and the peak count rates cluster around 2 Crab. The C_{min} and C_{max} distributions can be fitted by a single-Gaussian function, $f(x) = a_1 e^{-\left(\frac{x-b_1}{c_1}\right)^2}$, where a_1 , b_1 , and c_1 are fitting parameters. Alternatively, the double-Gaussian function ($f(x) = a_1 e^{-\left(\frac{x-b_1}{c_1}\right)^2} + a_2 e^{-\left(\frac{x-b_2}{c_2}\right)^2}$) provides better fittings to the distributions

¹ https://heasarc.gsfc.nasa.gov/docs/xte/recipes/stdprod_guide.html

² https://heasarc.gsfc.nasa.gov/docs/xte/recipes/ml1c_start.html to account for the degradation of detection efficiency (Figure 1)

of T_{rec} , *Amplitude*, and *Fluence* according to the F-test estimation (with a significance level above 99.9%). The fitting results are shown in Table 1 and Figure 2. The bimodal distributions of T_{rec} and *Fluence* are responsible for the two branches having a small apparent inner disk radius ($R_{\text{in}} \leq 70$ km) and a large one ($R_{\text{in}} > 70$ km, Figure 5, Section 3.2), respectively. The branch with smaller R_{in} typically has smaller C_{min} , *Fluence*, and shorter T_{rec} (see also Figure 3), and vice versa.

Mineo et al. (2016) investigated two long *BeppoSAX* pointings, and suggested that the minimum count rate was proportional to the one-third power of the recurrence time (see also Massaro et al. 2010). Here, we calculate the Spearman's rank correlation coefficient of $\rho/P = 0.70/0$ between C_{min} and T_{rec} , confirming their positive correlation. When fitted with a power-law function ($C_{\text{min}} = a T_{\text{rec}}^n$), we obtain an exponent of $n = 0.49 \pm 0.04$ and $a = 0.076 \pm 0.010$. Since the maximum count rate remains nearly constant, the amplitude ($C_{\text{max}}/C_{\text{min}}$) is anti-correlated with the C_{min} (Figure 3), which agrees with the results reported in Naik et al. (2002). The fluence is correlated with T_{rec} and is anti-correlated with the amplitude. Here, we also try to define the heartbeat cycle as the time between the minimum count rate. Because all of the structure parameters do not change much within an individual observation, the results derived in this way remain unchanged.

Examples of light curve with different recurrent time scales are displayed in Figure 4, in which the correlations described above are obvious. It can be also found that the change of the recurrent time is mainly because of the variation of rising time scale, namely from the C_{min} increasing to the C_{max} . In contrast, the decaying time scales (i.e. from C_{max} to C_{min}) are similar for different values of T_{rec} .

3.2. Spectral parameters

The spectral fitting results are presented in Figure 5. The unabsorbed power-law luminosity (L_{PL}) and the disk luminosity increase simultaneously with the total luminosity ($L_{3-30 \text{ keV}}$). The apparent inner disk radius (R_{in}) is related to the disk normalization as $N_{\text{disk}} = \frac{1}{f^4} \left(\frac{R_{\text{in}}}{D_{10}}\right)^2 \cos \theta$, where D_{10} is the distance in units of 10 kpc. Here we adopt an the inclination angle $\theta = 66^\circ$ (Fender et al. 1999), a color correction factor $f = 1.9$ (Nielsen et al. 2011), and a distance of 8.6 kpc (Reid et al. 2014) in the calculation. There are two branches shown in the diagrams of $L_{3-30 \text{ keV}} - R_{\text{in}}$ and $L_{3-30 \text{ keV}} - kT$: (1) The inner disk keeps at a small radius ($R_{\text{in}} \leq 70$ km, hereafter S branch), kT increases with the X-ray luminosity, and the X-ray emissions are fainter and softer (larger Γ). (2) The majority of data (189 out of 233) draw the other branch (L branch), the apparent inner edge of disk recedes and the temperature increases slowly at the high luminosity. Meanwhile, the photon index (Γ) of non-thermal component is anti-correlated with the X-ray luminosity.

Intriguingly, there are the positive correlations between T_{rec} , R_{in} and the X-ray luminosity as well. Additionally, T_{rec} has even tighter correlation with the power-law luminosity. Since the uncertainty on T_{rec} is much larger than on $L_{3-30 \text{ keV}}$, we carry out a power-law fit to $T_{\text{rec}} \propto L_{3-30 \text{ keV}}^n$ relation by taking the error on T_{rec} into

account, yielding an index of $n = 1.10 \pm 0.10$. Meanwhile, T_{rec} is proportional to $L_{\text{PL}}^{1.66 \pm 0.09}$.

It is worth to note that the change of apparent inner disk radius can be interpreted as a varying color correction factor without moving the intrinsic inner disk radius (e.g. Merloni et al. 2000; Zoghbi et al. 2016). In order to check this scenario, we model the disk component with *diskpn* (Gierliński et al. 1999), in which the disk normalization is linked to the color correction factor: $Norm_{\text{diskpn}} = \frac{M^2 \cos \theta}{D^2 f^4}$. The inner disk radius is fixed to the bottom limit $6 R_g$, although it is much smaller due to highly spinning (McClintock et al. 2006). In addition, the power-law model is replaced by a physical Comptonization model (*tbabs*(diskpn+comptt)* in XSPEC). We tie the seed temperature (kT_{seed}) to the disk temperature, and fix the plasma temperature to 50 keV because it cannot be constrained by our data. The data in the S branch are relatively soft, and the model described above cannot provide an adequate fit to them unless the kT_{seed} varies freely and becomes hotter than the disk temperature; however, it is inconsistent. Henceforth, we only fit the data in the L branch. With the X-ray luminosity increasing, the optical depth decreases, while the contribution of Comptonized component and the $Norm_{\text{diskpn}}$ increase (Figure 7). That is, the color correction factor decreases with the X-ray luminosity. Further discussion is presented in next section.

4. DISCUSSION & CONCLUSION

4.1. Movable accretion disk?

Plenty of works had been carried out to study the heartbeat state by investigating the individual observation (e.g. Massaro et al. 2010; Nielsen et al. 2011, 2012; Zoghbi et al. 2016; Yan et al. 2017, 2018). The regular flares are generally attributed to the thermal-viscous instability (i.e. the Lightman-Eardley instability, Lightman & Eardley 1974) when the inner region is dominated by radiation pressure at high luminosities (e.g. Belloni et al. 1997; Janiuk & Czerny 2005; Grzędzielski et al. 2017). Phenomenologically, the burst sequence could be interpreted as the rapid emptying of inner portion of the accretion disk, followed by a slower refilling the inner region, and it finishes a cycle on the viscous time scale (Belloni et al. 1997). Theoretically, some groups successfully reproduced the oscillating light curve with the proper cycle and the burst amplitude by modifying the classical description of α viscosity (e.g. Honma et al. 1991; Szuszkiewicz & Miller 1998; Merloni & Nayakshin 2006; Zheng et al. 2011; Grzędzielski et al. 2017). However, such models cannot account for the growth of R_{in} at the slow rise stage as suggested by the phase-resolved study (Nielsen et al. 2011). Moreover, our statistical analysis find the anti-correlation between T_{rec} and the amplitude (Figure 3), which is in contrast to the prediction of the modified viscosity model (Grzędzielski et al. 2017).

Besides the radiation pressure instability, Nielsen et al. (2011) argued that a local Eddington effect (Fukue 2004; Heinzeller & Duschl 2007) is required to explain some X-ray properties of the heartbeat state. When the luminosity is larger than the critical value ($\sim 0.3 - 1 L_{\text{Edd}}$), the radiation pressure could either push the disk outward or generate the optically thick out-

Table 1

	a_1	b_1	c_1	a_2	b_2	c_2
C_{\max}	15.4 ± 2.2	1.98 ± 0.01	0.22 ± 0.02	—	—	—
C_{\min}	10.8 ± 1.2	0.56 ± 0.01	0.25 ± 0.02	—	—	—
T_{rec}	20.4 ± 2.3	45.9 ± 0.8	9.4 ± 1.4	7.1 ± 0.8	72.8 ± 4.9	39.4 ± 4.2
<i>Fluence</i>	23.0 ± 2.5	41.1 ± 1.5	13.6 ± 3.1	5.9 ± 1.4	72.5 ± 19.1	58.3 ± 15.3
<i>Amplitude</i>	13.3 ± 2.0	2.96 ± 0.04	0.25 ± 0.07	5.7 ± 1.8	2.98 ± 1.15	2.4 ± 0.8

Note. — The distributions of C_{\max} and C_{\min} are fitted by a single-Gaussian function. On the other hand, those of T_{rec} , *Amplitude*, and *Fluence* are fitted by a double-Gaussian function.

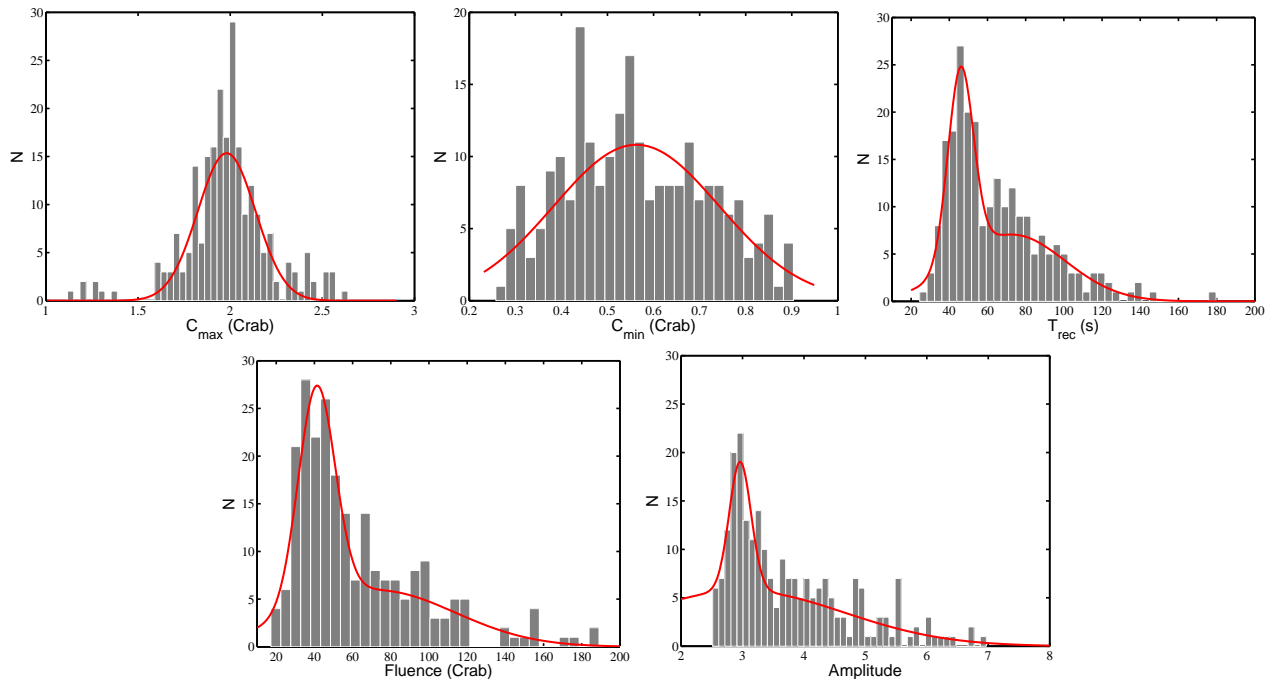


Figure 2. Distributions of the light curve structure parameters. We also apply either the single-Gaussian or double-Gaussian fitting to these distributions (red lines, Table 1).

flows (e.g. Poutanen et al. 2007; Weng et al. 2014; Urquhart & Soria 2016), or the disk might become thick and block the inner region (e.g. McClintock et al. 2006; Gu 2012). As a result, the apparent size of thermal component increases with the luminosity, and the X-ray emissions become harder in the meantime (Soria 2007; Middleton et al. 2015). In the S branch, the X-ray luminosity is below and close to the critical luminosity, softer emissions and smaller apparent accretion disk are observed. If the recurrence time of heartbeat flare is related to the viscous time of inner disk radius, we would expect that T_{rec} increases with increasing R_{in} and the X-ray luminosity as shown in Figure 6.

4.2. Variable corona?

The advection, coronal dissipation, and outflows play important roles in the stabilization of accretion flows at the high luminosity state (e.g. Janiuk et al. 2002). Investigating the quasi-simultaneous radio and X-ray data, Vadawale et al. (2003) achieved the association between jet and corona. For instance, the central Compton cloud (corona) is ejected during the soft X-ray dips, which are preceded by a radio-loud hard state. They argued that the change in the corona can account for the X-ray variations that were previously attributed to the accretion disk. Such scenario, in particular, is supported

by the absence of both the Comptonized component and low-frequency QPOs during the X-ray dips. Note that low-frequency QPO signals detected in low-mass X-ray binaries are generally connected with the hard component but not (or sometimes indirectly linked with) the thermal accretion disk (e.g. Belloni & Stella 2014; Motta et al. 2015; Zhao et al. 2016; Zhang et al. 2017; Yan et al. 2018).

Our results indicate that, for observations with different T_{rec} , the main difference is from the slow rise stage, while the source takes almost the same time to return from the peak luminosity to the minimum (Figure 4). The change of C_{\min} would further point to the variation of corona and jet properties for different T_{rec} oscillations. The tighter correlation between R_{in} and the power-law luminosity (Figure 6) also supports that the limit cycle is driven by the non-thermal emissions rather than the thermal component. Meanwhile, C_{\max} remains nearly constant, indicating that the bolometric luminosity of GRS 1915+105 reaches its Eddington luminosity.

The variation of corona does not only affect the Comptonized component itself, but also modify the property of observed disk thermal emission via Compton scattering (e.g. Shimura & Takahara 1995; Nayakshin et al. 2000). The spectral hardening factor f is by no means constant as we assumed in the R_{in} calculation. It should

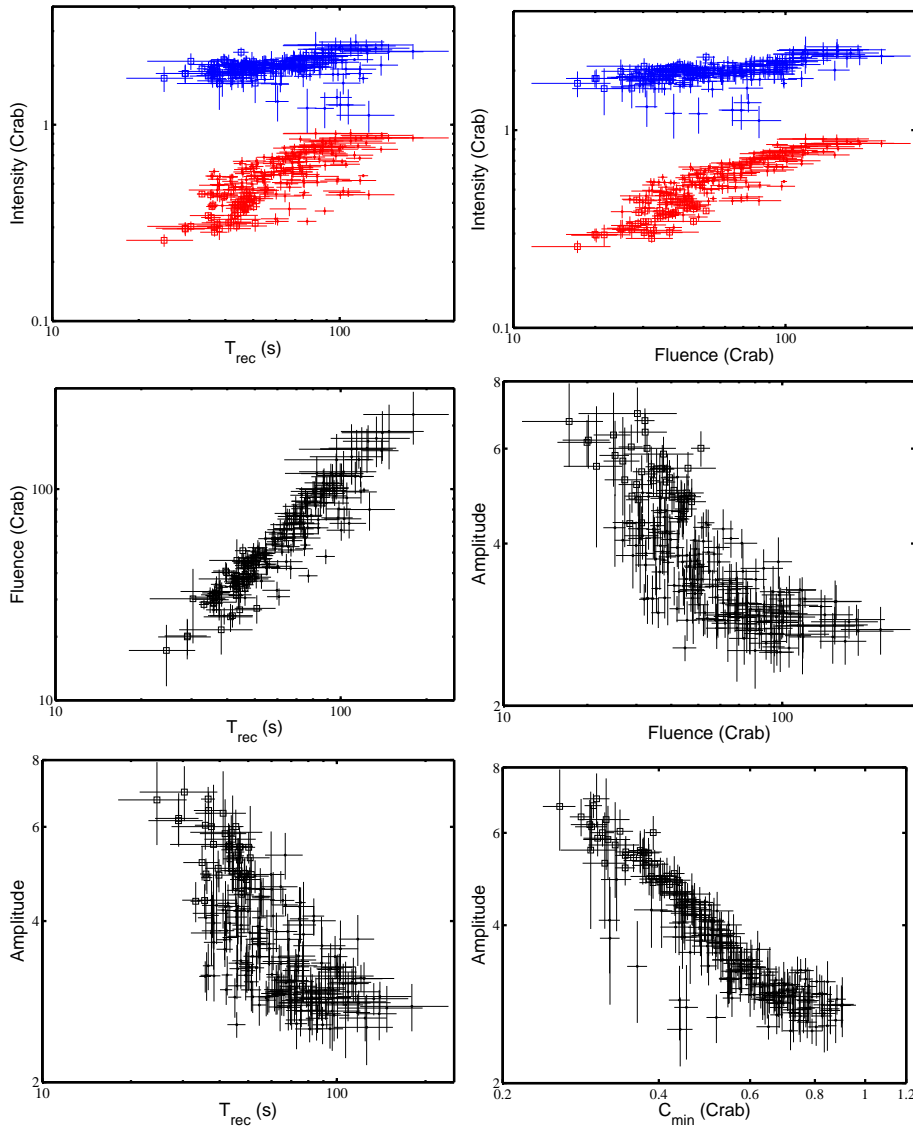


Figure 3. Correlations between the structure parameters of light curves. In the top two panels, the red and blue points correspond to C_{\min} and C_{\max} , respectively. In this work, open squares and filled cycles mark the data with the apparent inner radius being smaller and larger than 70 km (Figure 5), respectively.

depend on the accretion rate, the fraction of the accreted power released in the corona, the corona reflecting, etc (e.g. Merloni et al. 2000; Davis et al. 2005). When the actual inner boundary of accretion disk is fixed, the color disk radius could vary by more than a factor of 4 with different accretion parameters (Merloni et al. 2000).

Additionally, Zoghbi et al. (2016) argued that a change in composition of disk atmosphere could make even larger change in the color correction factor. As the disk temperature and flux increase, more iron ions are elevated up by the radiation force, increasing the opacity in the upper disk and resulting in smaller f . They further suggested that the evolution of R_{in} inferred from the disk blackbody component was artificial, while the actual inner edge kept at a small radius ($\sim 1.1 R_g$) in the heartbeat state according to the reflection measurement. Specifically, Zoghbi et al. (2016) proposed that the inner disk radius remained constant and the corona changed size during oscillations. If the corona is smaller and closer to the central BH, more photons are dragged by the strong

gravity and hit the disk; therefore, less photons can reach observer. This model is in qualitative agreement with our results presented in Figure 7, i.e. the *comptt*-to-total-flux ratio and T_{rec} increase with the total X-ray luminosity. The change of apparent disk size shown in Figure 5 can be interpreted as the variation of color correction factor. The correlation between the X-ray/disk flux and $Norm_{\text{diskpnp}}$ (Figure 7) indicates that the factor f decreases from ~ 3.0 to ~ 2.4 with the increasing luminosity. But note that the inner disk radius was fixed to $6 R_g$, the actual value of f would be smaller with smaller inner disk radius.

Although the varying corona scenario offers promising explanation for the results given by our statistical analysis, we cannot completely rule out the evolving disk model. In addition, a number of questions remain to be answered. (1) What is the origin of variations in the corona (and the disk)? (2) If the low-frequency QPOs and T_{rec} are account for different time scales of corona, e.g. dynamical time and thermal/viscous time; but their

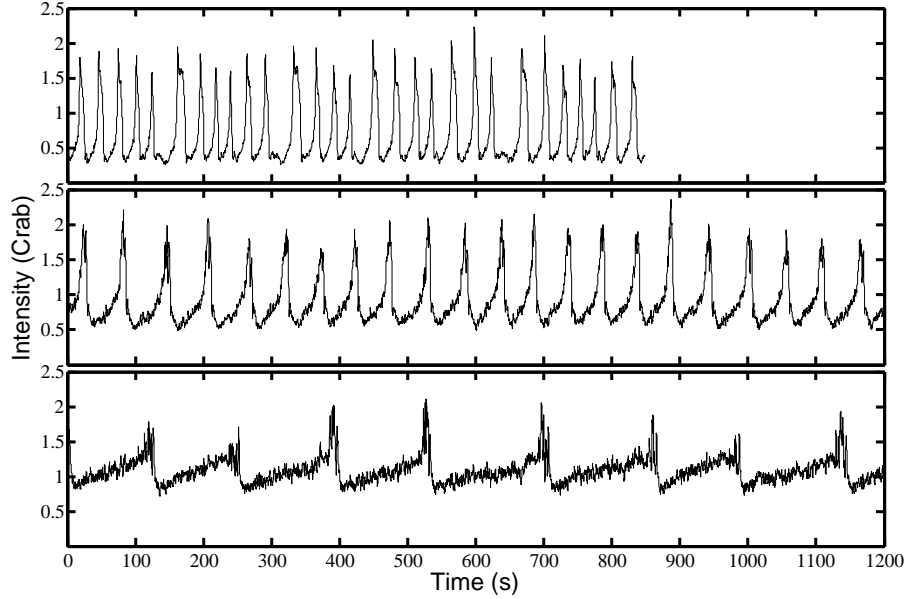


Figure 4. Examples of light curve for different recurrent time scales. The data come from observations 92702-01-14-00 ($R_{\text{in}} = 63.8^{+2.4}_{-2.3}$ km, upper panel), 95701-01-03-00 ($R_{\text{in}} = 87.5^{+2.1}_{-2.7}$ km, middle panel), and 91701-01-52-01 ($R_{\text{in}} = 91.5^{+2.7}_{-2.7}$ km, bottom panel), respectively.

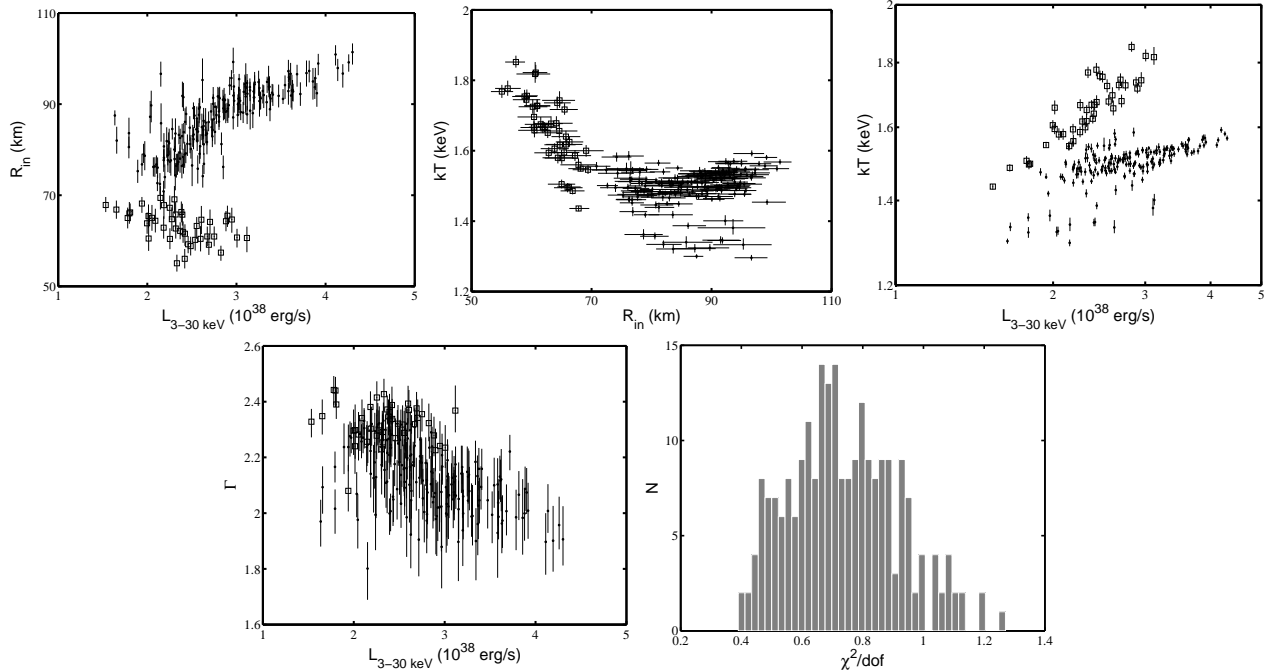


Figure 5. Correlations between the spectral parameters and distribution of the reduced χ^2 with the fitting model of *diskbb+powerlaw* (right bottom panel). Open squares and filled cycles correspond to the data with R_{in} being smaller and larger than 70 km, respectively. All parameters are plotted with their 1σ errors.

correlation is unknown at current stage. (3) It had been pointed out that the reflection component is prominent in the heartbeat state (Zoghbi et al. 2016). The evolution trend of disk component and the total X-ray luminosity are insensitive to models with or without the reflection. However, the parameters of the thermal and Comptonization components might change when the reflection is included or excluded in fitting models. Unfortunately, we cannot study the reflection spectrum with the *RXTE*/*PCA* data due to its low energy resolution.

On the other hand, the single *Nustar* observation is inadequate to explore the spectral/temporal evolution with different T_{rec} . Thus, we would like to suggest that multiple high quality data (high energy/time resolution) from *Insight-HXMT* and *Nustar* are required to probe the peculiar state deeper.

We thank the referee for helpful comments and suggestions. We thank Drs. Shu-Ping Yan, Ming-Yu Ge and You-Li Tuo for many valuable suggestions. This work is

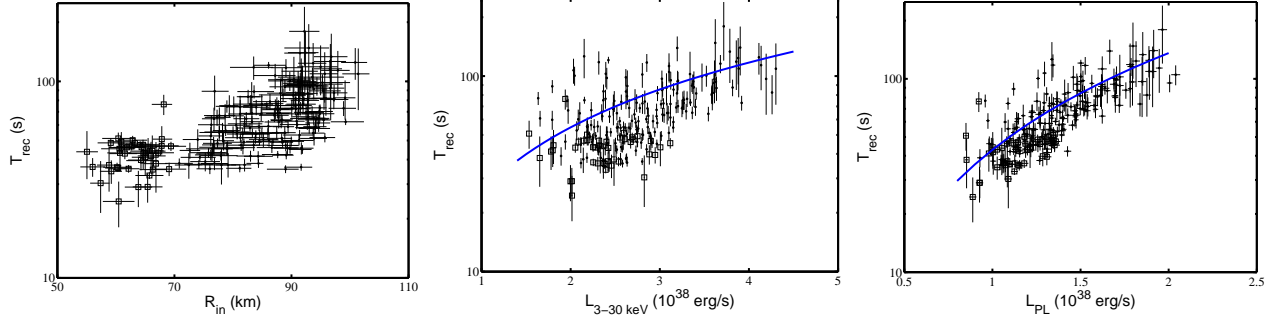


Figure 6. Recurrence time increases with R_{in} , $L_{3-30 \text{ keV}}$, and L_{PL} . The power-law function is employed to fit the $L_{3-30 \text{ keV}} - T_{rec}$ and $L_{PL} - T_{rec}$ correlations (blue lines).

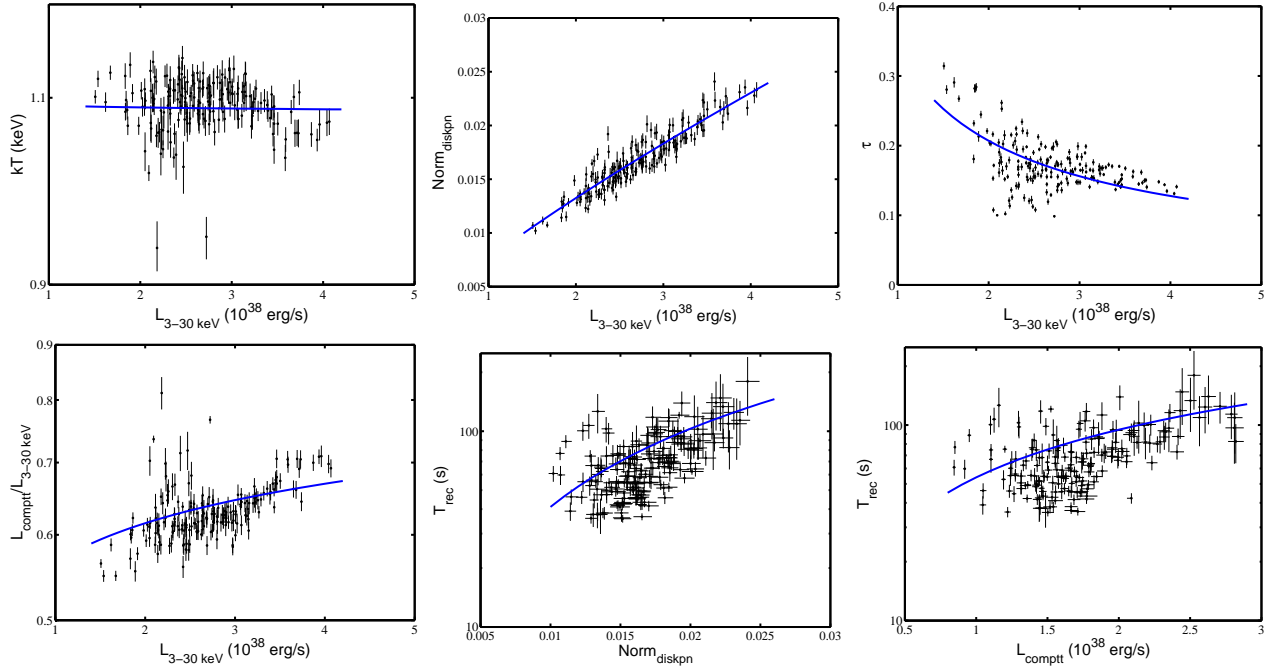


Figure 7. Correlations between the spectral parameters of *diskpn+comptt* model and the structure parameters of light curves. Blue lines correspond to the power-law fittings: $kT \propto L_{3-30 \text{ keV}}^{0.00 \pm 0.01}$, $Norm_{diskpn} \propto L_{3-30 \text{ keV}}^{0.80 \pm 0.03}$, $\tau \propto L_{3-30 \text{ keV}}^{-0.70 \pm 0.06}$, $L_{comptt}/L_{3-30 \text{ keV}} \propto L_{3-30 \text{ keV}}^{0.12 \pm 0.03}$, $T_{rec} \propto Norm_{diskpn}^{1.38 \pm 0.11}$, and $T_{rec} \propto L_{comptt}^{0.81 \pm 0.08}$.

supported by the National Natural Science Foundation of China under grants 11673013, 11703014, 11433005, and 11573023, and the Natural Science Foundation from Jiangsu Province of China (Grant No. BK20171028).

Facilities: *RXTE*

Software: HEASOFT.

REFERENCES

- Arnaud, K. A. 1996, in *Astronomical Society of the Pacific Conference Series, Vol. 101, Astronomical Data Analysis Software and Systems V*, ed. G. H. Jacoby & J. Barnes, 17
- Altamirano, D., Belloni, T., Linares, M., et al. 2011, *ApJL*, 742, L17
- Belloni T. M., & Altamirano D., 2013, *MNRAS*, 432, 19
- Belloni, T., Klein-Wolt, M., Méndez, M., van der Klis, M., & van Paradijs, J. 2000, *A&A*, 355, 271
- Belloni, T. M., & Stella, L. 2014, *SSRv*, 183, 43
- Belloni, T., Méndez, M., King, A. R., van der Klis, M., & van Paradijs, J. 1997, *ApJL*, 479, L145
- Blum, J. L., Miller, J. M., Fabian, A. C., et al. 2009, *ApJ*, 706, 60
- Castro-Tirado, A. J., Brandt, S., & Lund, N. 1992, *IAU Circ.*, 5590, 2
- Court, J. M. C., Altamirano, D., Pereyra, M., et al. 2017, 468, 4748
- Davis, S. W., Blaes, O. M., Hubeny, I., & Turner, N. J. 2005, *ApJ*, 621, 372
- Fender, R., & Belloni, T. 2004, *ARA&A*, 42, 317
- Fender, R. P., Gallo, E., & Russell, D. 2010, *MNRAS*, 406, 1425
- Fender, R. P., Garrington, S. T., McKay, D. J., et al. 1999, *MNRAS*, 304, 865
- Fukue, J. 2004, *PASJ*, 56, 569
- Gierliński, M., Zdziarski, A. A., Poutanen, J., et al. 1999, *MNRAS*, 309, 496
- Greiner, J., Cuby, J. G., McCaughrean, M. J., Castro-Tirado, A. J., & Mennickent, R. E. 2001, *A&A*, 373, L37
- Grzędzielski, M., Janiuk, A., Czerny, B., Wu, Q. 2017, *A&A*, 603, 110
- Gu, W.-M. 2012, *ApJ*, 753, 118
- Hannikainen, D. C., Rodriguez, J., Vilhu, O., et al. 2005, *A&A*, 435, 995
- Heinzeller, D., & Duschl, W. J. 2007, *MNRAS*, 374, 1146
- Honma, F., Kato, S., & Matsumoto, R. 1991, *PASJ*, 43, 147
- Janiuk, A., Czerny, B., & Siemiginowska, A. 2002, *ApJ*, 576, 908
- Janiuk, A., & Czerny, B. 2005, *MNRAS*, 356, 205
- Klein-Wolt, M., Fender, R. P., Pooley, G. G., Belloni, T., Migliari, S., Morgan, E. H., & van der Klis, M. 2002, *MNRAS*, 331, 745

- Lee, J. C., Reynolds, C. S., Remillard, R., et al. 2002, *ApJ*, 567, 1102
- Lightman, A. P., & Eardley, D. M. 1974, *ApJL*, 187, L1
- Massaro, E., Ventura, G., Massa, F., Feroci, M., Mineo, T., Cusumano, G., Casella, P., & Belloni, T. 2010, *A&A*, 513, A21
- McClintock, J. E., Shafee, R., Narayan, R., Remillard, R. A., Davis, S. W., & Li, L.-X. 2006, *ApJ*, 652, 518
- Merloni, A., Fabian, A. C., & Ross, R. R. 2000, *MNRAS*, 313, 193
- Merloni, A., & Nayakshin, S. 2006, *MNRAS*, 372, 728
- Middleton, M., Done, C., Gierliński, M., & Davis, S. W. 2006, *MNRAS*, 373, 1004
- Middleton, M. J., Heil, L., Pintore, F., Walton, D. J., & Roberts, T. P. 2015, *MNRAS*, 447, 3243
- Miller, J. M., Parker, M. L., Fuerst, F., et al. 2013, *ApJL*, 775, L45
- Mineo, T., Massa, F., Massaro, E. & D’Aì, A. 2016, *A&A*, 586, A56
- Mirabel, I. F. & Rodríguez, L. F. 1994, *Nature*, 371, 46
- Morgan, E. H., Remillard, R. A., & Greiner, J. 1997, *ApJ*, 482, 993
- Motta, S. E., Casella, P., Henze, M., et al. 2015, *MNRAS*, 447, 2059
- Naik, S., Agrawal, P. C., Rao, A. R., Paul, B., 2002, *MNRAS*, 330, 487
- Narayan, R. & McClintock, J. E. 2012, *MNRAS*, 419, L69
- Nayakshin, S., Rappaport, S., & Melia, F. 2000, *ApJ*, 535, 798
- Neilsen, J., Remillard, R. A., & Lee, J. C. 2011, *ApJ*, 737, 69
- . 2012, *ApJ*, 750, 71
- Poutanen, J., Lipunova, G., Fabrika, S., Butkevich, A. G., & Abolmasov, P. 2007, *MNRAS*, 377, 1187
- Reid, M. J., McClintock, J. E., Steiner, J. F., Steeghs, D., Remillard, R. A., Dhawan, V., & Narayan, R. 2014, *ApJ*, 796, 2
- Shimura, T., & Takahara, F. 1995, *ApJ*, 445, 780
- Soria, R. 2007, *Ap&SS*, 311, 213
- Szuskiewicz, E., & Miller, J. C. 1998, *MNRAS*, 298, 888
- Urquhart, R., & Soria, R. 2016, *MNRAS*, 456, 1859
- Vadawale, S. V., Rao, A. R., Naik, S., et al. 2003, *ApJ*, 597, 1023
- Weng, S.-S., Zhang, S.-N., & Zhao, H.-H. 2014, *ApJ*, 780, 147
- Yadav, J. S., Rao, A. R., Agrawal, P. C., Paul, B., Seetha, S., & Kasturirangan, K. 1999, *ApJ*, 517, 935
- Yan, S.-P., Ji, L., Méndez, M., Liu, S.-M., Wang, N. et al. 2017, *MNRAS*, 465, 1926
- Yan, S.-P., Ji, L., Liu, S.-M., Méndez, M., Wang, N. et al. 2018, *MNRAS*, 474, 1214
- Zdziarski, A. A., Gierliński, M., Rao, A. R., Vadawale, S. V., & Miłkołajewska, J. 2005, *MNRAS*, 360, 825
- Zhang, L., Chen, L., Qu, J.-L., & Bu, Q.-C. 2015, *AJ*, 149, 82
- Zhang, S. N., Cui, W., & Chen, W. 1997, *ApJL*, 482, L155
- Zhang, L., Wang, Y., Méndez, M., et al. 2017, *ApJ*, 845, 143
- Zhao, H.-H., Weng, S.-S., Qu, J.-L., Cai, J.-P., & Yuan, Q.-R. 2016, *A&A*, 593, A23
- Zheng, S.-M., Yuan, F., Gu, W.-M., & Lu, J.-F. 2011, *ApJ*, 732, 52
- Zoghbi, A., Miller, J. M., King, A. L., et al. 2016, *ApJ*, 833, 165